Research paper

Real-time analysis of decomposed gas from HAN(aq.) with/without Ir-based catalyst by thruster-simulation/MPI/TOF-MS

Noboru Itouyama*†, Totaro Imasaka**, and Keiichi Hori***

*Department of Chemical System Engineering, Graduate School of Engineering, The University of Tokyo, 7–3–1 Hongo, Bunkyo–ku, Tokyo, 113–8654 JAPAN
Phone: +81–050–3362–5674
†Corresponding author: itouyama.noboru@ac.jaxa.jp

**Division of International Strategy, Center for Future Chemistry, Kyushu University, 744 Motooka, Nishi–ku, Fukuoka–shi, Fukuoka, 819–0395 JAPAN

***JAXA (ISAS), Japan Aerospace Exploration Agency (Institute of Space and Astronautical Science), 3–1–1 Yoshinodai, Chuo–ku, Sagamihara–shi, Kanagawa, 252–0222 JAPAN

Received: March 6, 2017 Accepted: April 19, 2018

Abstract

Using multiphoton ionization/time-of-flight mass spectrometry, we evaluated the validity of the conventional mechanism for thermal decomposition of hydroxylammonium nitrate (HAN) and investigated the corresponding catalytic reaction to determine the decomposed gases in real time, through a pathway that models a real thruster. HAN with a hot catalyst can provide a low-toxicity, high-performance alternative to hydrazine for use in thruster systems. Our results show that the decomposition of HAN mostly follows the conventional model, but some further reactions need to be considered. We found that the catalyst facilitated the reaction of NH_2OH with HONO in the catalytic reaction of HAN and propose a new decomposition pathway.

Keywords: reaction control system (RCS), hydroxylammonium nitrate (HAN), catalyst, time-of-flight mass spectrometry, multiphoton ionization (MPI)

1. Introduction

It is important to achieve high accuracy and reliability in reaction control systems (RCSs). A conventional thruster is required to respond rapidly, with high impulse reproducibility over a long life cycle.

To date, the most well-known propellant for use in RCS thrusters has been hydrazine[1]. Hydrazine is easy to decompose with a catalyst at room temperature. For this reason, hydrazine thrusters are highly responsive and show high performance reproducibility. On the other hand, hydrazine has some disadvantages such as high toxicity and carcinogenicity, which makes it difficult to handle, and its high freezing point requires the use of a heater in deep space probes. As a result, green propellants (GPs) such as hydroxylammonium nitrate (HAN, NH_3OH-NO_3) have been studied widely since the 1990s[2]. HAN is easy to handle because of its low toxicity and low freezing point. In addition, it has a higher density and specific impulse (I_{sp}) than hydrazine[3].

As is the case for hydrazine, impulse in a monopropellant thruster occurs through the decomposition and burning of HAN on a catalyst surface. From the viewpoint of safety and performance, it is important that we are able to simulate the temperature, pressure, and gas concentration profiles of the thruster. Unfortunately, there have been few reports on the HAN-catalyst reaction mechanism. It is therefore necessary to investigate the mechanism of this reaction further. The HAN-catalyst reaction model is based on the thermal decomposition model of Lee et al.[4], in which decomposed

Table 1 Comparison of the characteristics of hydrazine and SHP163.

		SHP163	Hydrazine
Density [g cc^{-1}] @20°C		1.4	1.0
Freezing point [°C]		≤30	1.4
Specific impulse [s]*		276	233
Adiabatic flame temperature [K]*		2394	871
Toxicity	LD50 oral [mg kg^{-1}]	300~2000	60
	LD50 transdermal [mg kg^{-1}]	>2000	91

*Conditions: $P_c = 0.7$[MPa], $A_e/A_t = 50$.

gases owing to the high-speed heating of aqueous HAN at several concentrations were analyzed by Fourier transform infrared spectroscopy (FT-IR), leading to calculation of reaction rate constants by inverse analysis[4]. The chemical kinetics is different in an actual thruster, in which the propellant is sprayed into a hot catalyst. Therefore, before constructing a comprehensive combustion model, it is necessary to evaluate the validity of the reported reaction model and its applicability to the catalyzed reaction. The first step in elucidating the HAN-catalyst reaction mechanism in a thruster is to compare existing reports of related thermal decomposition reactions with results from real-time gas analyses of the same reactions in a simulated thruster.

We studied a monopropellant thruster with HAN as the propellant, with and without catalysts, in order to determine their benefit[5),6)]. SHP163 is a HAN propellant that consists of 73.6 wt.% HAN, 6.2 wt.% H_2O, 3.9 wt.% ammonium nitrate (AN), and 16.3 wt.% methanol. Table 1 compares the characteristics of the HAN propellant (SHP 163) with those of hydrazine.

Spectroscopic analysis of the burned gas is an affordable method of investigating the reaction mechanism. Klein[7)] and Schoppelrei[8)] reported the FT-IR analysis of the decomposed gas from a HAN solution, and Schoppelrei[9)] analyzed gases from the thermal decomposition of aqueous HAN by Raman spectroscopy. In all of these reports, the decomposed gas was generated at a lower heating rate like thermogravimetry-differential thermal analysis (TG-DTA). However, in actual thruster tests, we kept the test chamber under vacuum. Use of a laser as the light source during spectroscopic analysis is popular. Unfortunately, our thruster test conditions make this type of spectroscopic analysis difficult, mainly because of the scale of the experiment. It is important to analyze the decomposed gas in real time at laboratory scale for a similar reaction pathway as that of a real thruster. One solution is to use FT-IR. The IR spectrum depends on the polarizability of a given molecule[10)]. For molecules that have structural symmetry, such as N_2 or O_2, no IR peaks will be observable because of the loss of infrared activity[11)]. Likewise, in the case of Raman spectroscopy, Raman scattering is difficult to observe as its intensity is 10^{-6} times weaker than that of Rayleigh scattering[12)]. Consequently, a characterization method that provides the minimal number of peaks while encompassing all reaction information would be useful. With this background in mind, we considered the possibility of using time-of-flight mass spectrometry (TOF-MS) for real-time analysis. TOF-MS makes it possible to use peaks corresponding to the molecular weights of the various products during analysis.

We considered using TOF-MS analysis on our (downsized) laboratory-scale simulated thruster reaction pathway. In this experiment, it is essential that minimal fragmentation occurs following ionization; otherwise only fragment peaks will be observed during analysis. In conventional MS, electron impact (EI) ionization is one of the most popular methods employed. The main disadvantage of EI is that it is often accompanied by significant amounts of fragmentation[13)]. HNO_3 is one of the decomposition products from HAN that shows significant fragmentation using EI/MS[14)]. Therefore, to overcome this problem, we selected multiphoton ionization (MPI) as a relatively soft ionization method. Imasaka et al. used MPI/TOF-MS for the sensitive analysis of toxic compounds, such as dioxine[15)]. These researchers also studied the effect of pulse length. In the MPI step, photon density affects ionization efficiency. A femtosecond pulse was reported to be ten times more sensitive than that a picosecond pulse when applied to the analysis of pentachlorodibenzofuran[16)]. This technique was not only applied to toxic compounds, they also reported high sensitivity for the analysis of explosives such as triacetone triperoxide (TATP)[17)], hexamethylenetriperoxidediamine (HMTD)[18)], trinitrotoluene (TNT)[18)], and trimethylenetrinitramine (RDX)[18)], which are known to be difficult to detect using conventional MPI/TOF-MS analysis because of their instability. In the analysis of TATP, using molecular ion peaks, this method was shown to have a detection limit of the order of 10 pg, while other methods that focus on fragment peaks had detection limits at the 10−100 pg level. By controlling the photon energy (wavelength) as a method of adjusting ionization energy, molecular ion peaks for HMTD and TNT could be found during their MPI/TOF-MS analyses. In addition, a comprehensive analysis of nitrated polycyclic aromatic hydrocarbons (NPAHs), which were reported to fragment strongly[19),20)] during conventional analysis, showed molecular ion peaks.

In MS analysis, it is usual to use gas chromatography (GC) to separate samples between the inlet and the TOF-MS parts of the instrument. In this study, we added a glass tube to the inlet and placed the catalyst into it. This system simulates the pathway of a thruster. In addition, we removed the GC system, and made the following modifications to prevent possible secondary reactions during transport of the product gases: (1) the inlet and TOF-MS were connected with the shortest possible length of inert silica capillary; (2) transport was made adiabatic by maintaining a constant temperature (300 °C) from the inlet to the entrance of TOF-MS.

In this paper, we detail our MPI/TOF-MS analyses of HAN samples that were subjected to several thruster simulation conditions, as shown in Figure 1. From these results, we discuss the HAN thermal decomposed model,

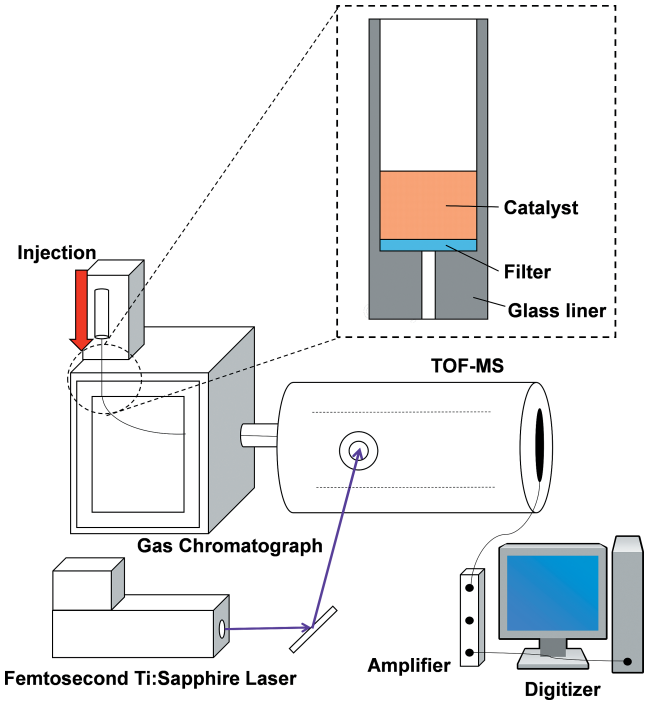

Figure 1 Thruster-simulation/MPI/TOF-MS.

as well as investigating the catalyst reaction model.

2. Experimental

2.1 Sample preparation

Decomposition of aqueous HAN (HAN 95 wt.%, H_2O 5 wt.%, Hosoya Pyro) in the absence of a catalyst[21] can require temperatures of up to 1100 K, and this may adversely affect the analysis equipment if an undiluted sample is injected directly. Consequently, we diluted our samples with acetonitrile (Wako Chemical), which was selected as the solvent because it provides the lowest background signals. From the viewpoint of reaction exothermicity within the equipment, and detection sensitivity, 100-fold dilution proved to be the best, and this dilution was used for all experiments.

2.2 Apparatus

Details of the analytical TOF-MS instrument are reported elsewhere[22)–24)]. The sample solution (1 μL) was injected into the GC (6890GC, Agilent Technologies, CA) using an autosampler (7683 B Series, Agilent Technologies). Helium, at a flow rate of 1 mL min^{-1}, was used as the carrier gas. A glass liner (Ultra-inert liner 5190 -2293, Agilent Technologies, CA) was installed at the GC inlet. This allowed for the selection of either thermal decomposition, or catalyst decomposition conditions, without, or with catalyst in the glass liner, respectively. In this study, the S405 catalyst was selected. S405 is an Ir-based catalyst that is popular in hydrazine thrusters. The eluted analytes were introduced into a linear-type TOF-MS (HGK-1, Hikari-GK, Fukuoka) through an inactive silica capillary transfer line (length, 1 m; inner diameter, 0.25 mm; Agilent Technologies). The outlet was heated to 150 °C to prevent clogging of the analytes at the end of capillary before injection into the TOF-MS. This ferrule temperature has been shown to be effective for the analysis of high energy materials[18)]. The GC temperature was set to the same temperature as the inlet, ensuring adiabatic gas transportation. In this paper, we employed two experimental temperatures, one at 300 °C, that mimicked the real initial temperature of the catalyst bed on thruster actuation, the other at 200 °C, which is higher than the decomposition temperature of HAN (~160 °C)[25)]. The third harmonic emission (267 nm, 90 μW) of a femtosecond Ti:sapphire laser (800 nm, 85 fs, 1 W, 1 kHz, Libra, Coherent, USA) was used as the ionization source. The induced ions were detected by microchannel plates (MCP; F4655-11, Hamamatsu Photonics, Shizuoka, Japan). After passing through an amplifier (Timing Amplifier 574, ORTEC, USA), the signal was recorded with a computer-interfaced digitizer (Acquiris AP 240, Agilent Technologies, CA). In the case of mass spectra, due to the removal of the GC, peaks from the eluted solvent, as background, were also recorded. For that reason, after acquiring the mass spectrum of the pure solvent, subsequent mass spectra were calculated as follows. Since the initial sample was diluted by a factor of 100, the resulting mixture is made up of 1% original sample and 99% solvent. Consequently, the solvent mass spectrum was multiplied by a factor 0.99 (99%) (Equation (1)). In this equation, I_c is the calibrated mass spectrum, I_R is the raw mass spectrum, and I_s is the solvent-only mass spectrum.

$$\sum_{i}^{m}\sum_{j}^{t} I_c[i,j] = \sum_{i}^{m}\sum_{j}^{t} I_R[i,j] - 0.99\sum_{i}^{m}\sum_{j}^{t} I_s[i,j] \quad (1)$$

Table 2 details the experimental conditions. All experiments were repeated three times.

Table 2 Analysis conditions.

Sample	HAN 95 3 [wt.%] + H_2O 5 [wt.%]
Dilution solvent	Acetonitrile
Dilution concentration	100 times
Injection volume	1 [μL]
Catalyst	with/without S405
Set temperature	200, 300 [°C]
Laser wavelength	267 [nm] (800 [nm] THG)
Capillary length	0.5 [m]
Carrier gas	He (1 [mL/min])

3. Results and discussion

3.1 Thermal decomposition model

Figure 2 is the reaction map of HAN decomposition by Lee[4)], it is the conventional thermal decomposition model. The mass spectrum resulting from the experiment conducted at 300 °C, without catalyst, is shown in Figure 3. Under these conditions, there were no differences between three different experiments indicating high reproducibility. Peaks at m/z 17, 18, 30, 32, 33, 46, and 74 are observed clearly. It is important to determine whether these peaks correspond to molecular ions themselves, or to fragment ions resulting from the fragmentation of decomposed gas molecules after ionization. In case of ions resulting from fragmentation with higher excess energies, it is well known that their peaks are broader, having wider

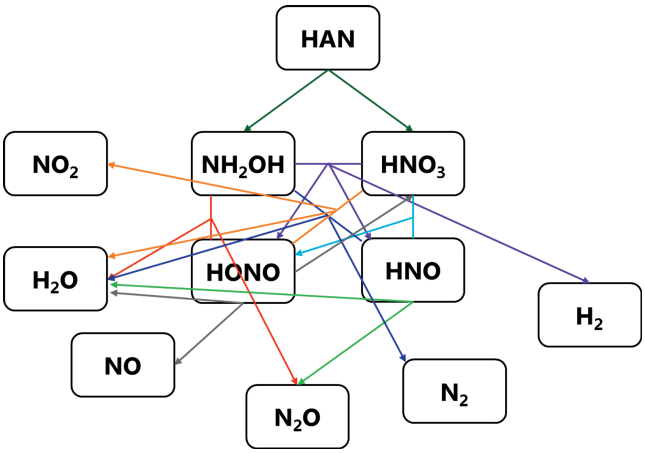

Figure 2 Reaction diagram by Lee[4].

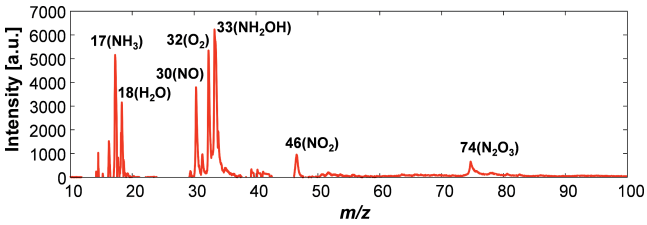

Figure 3 Mass spectrum of HAN (aq.)/acetonitrile at 300 °C without S405.

Table 3 FWHM of mass spectrum peaks.

m/z	FWHM [m/z]
17	0.32
18	0.18
30*	0.26*
32	0.28
33	0.34
46	0.41
74	0.55

*Reference

full widths at half maximum (FWHM). In this study, we chose the NO peak as a reference because it has a very simple chemical structure and is expected to have the smallest fragmentation of the decomposed gas species. We calculated the mass resolution of this TOF-MS instrument by measuring the FWHM of the NO peak and applying Equation (2).

$$\text{MassResolution} = \frac{m/z}{m/zFWHM} \quad (2)$$

By applying this formula, the mass resolution was determined to be about 180, and the FWHM of the NO peak was around 0.2. FWHM values for other peaks were obtained in a similar fashion and are summarized in Table 3. No peak was found to have a FWHM value that was significantly different to that of the reference. We can therefore conclude that all of the peaks observed in this experiment are most likely to be molecular ion peaks.

HAN contains nitrogen (N), hydrogen (H), and oxygen (O). When we compare our result with that of the conventional thermal decomposition model, we could assign the m/z 17 peak to NH_3, m/z 18 to H_2O, m/z 30 to

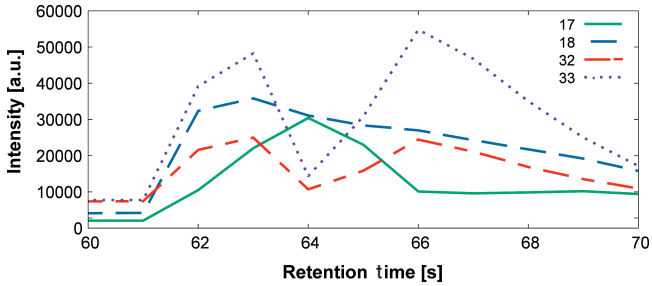

Figure 4 Chromatograms of the ions corresponding to m/z = 17, 18, 32 and 33 following HAN (aq.) decomposition at 300 °C without S405.

NO, m/z 32 to O_2, m/z 33 to NH_2OH, m/z 46 to NO_2, and m/z 74 to N_2O_3. Thus, new, unreported peaks were generated on deposition of HAN(aq.). However, we cannot ignore the fragmentation of the reaction products upon ionization in the mass spectrometer[26]. In other words, the m/z 17 peak can also arise because of the loss of H from H_2O (m/z 18), and the m/z 32 peak from the loss of H from NH_2OH (m/z 33). Therefore, we checked the chromatogram to identify these peaks. Figure 4 shows the chromatograms obtained, for peaks with m/z 17, 18, 32, and 33.

The shapes of the chromatograms for ions of m/z 17 and 18 are different. This means that m/z 17 most likely corresponds to the molecular ion peak of NH_3, and does not come from the loss of H from H_2O. Likewise, we compared m/z 32 and 33. They were similar in appearance, so it is possible that m/z 32 arises from the fragmentation of NH_2OH. However, it seems that the m/z 16 peak also appears in the mass spectrum of O_2 along with the m/z 32 peak. The peak corresponding to m/z 16 exhibited different behavior to that from m/z 33. One possibility is that m/z 32 corresponds to O_2, but it is necessary to discuss the identification of m/z 32 in greater detail. Next, we identified the m/z 74 peak, which is heavier than previously reported species and suggested an $N_xH_yO_z$ structure, so it seems most likely to be due to N_2O_3.

Reactions that produce N_2O_3 are very important in environmental chemistry[27),28], and are regarded to be the main reactions between NO and NO_2[29]. However, it has been reported that N_2O_3 forms structural isomers upon heating, or absorption of light[30]. This isomerization makes N_2O_3 more stable and causes the emergence of N_2O_3 peaks in mass spectra. As a consequence, we did not observe a peak at m/z 63 corresponding to HNO_3 (Figure 3) or it was generated at a volume below that of the detection limit. This result led us to analyze an ammonium nitrate (AN) sample (100-fold diluted with acetonitrile), which is expected to generate HNO_3 upon decomposition, in order to determine whether its absence in Figure 3 is a consequence of the detection limit of the analyzer, or its lack of formation. Figure 5 depicts the mass spectrum of the AN sample, which shows a very weak, but observable, peak at m/z 63. This result shows that the levels of HNO_3 produced during HAN decomposition falls below the detection limit of the analyzer. Instead, we found a strong peak around m/z 91-92. According to the mechanism of N_2O_3 generation during HAN decomposition, this strong peak corresponds to an adduct formed from product

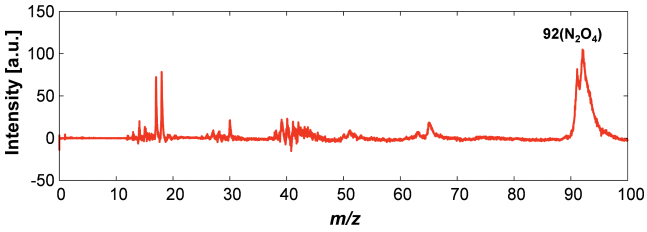

Figure 5 Mass spectrum of AN/acetonitrile (1:99) at 300 °C without catalyst.

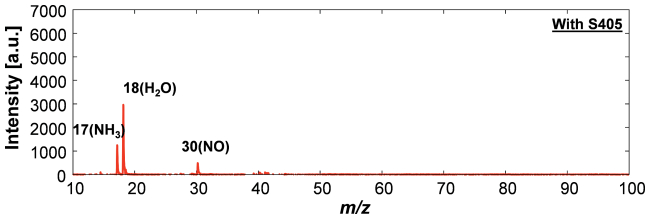

Figure 6 Mass spectrum of HAN (aq.)/acetonitrile at 300 °C with S405.

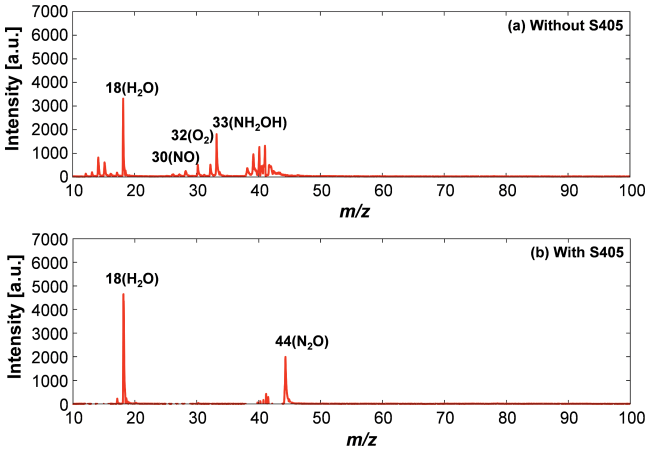

Figure 7 Mass spectra of HAN (aq.)/acetonitrile at 200 °C with/without S405; (a) without S405 catalyst; and (b) with S405 catalyst.

gases, such as NO_2+NO_2 or HNO_3+NO. During HAN decomposition, it has been reported that the NO concentration in the product gases is greater than that of NO_2[6]. For that reason, the peak at *m/z* 74 in Figure 3 might correspond to a product that is generated through the following steps: (1) NO_2 is produced and reacts rapidly with excess NO gas to form N_2O_3. (2) N_2O_3 gains energy from heat or light, and then (3) isomerizes to its structural isomer to gain higher stability. This mechanism predicts that the peak at *m/z* 92 in might correspond to the dimer, NO_2-NO_2. It is clearly important to consider this dimerization reaction in order to improve the reaction model.

In conclusion, the conventional model for the thermal decomposition of HAN has higher applicability and validity and can be extended to the catalyst decomposition model. On the other hand, it is important to investigate and add other reaction products into the model, in this case NH_3 or dimeric species such as NO_2-NO_2, for this extension to be valid.

3.2 Investigation into the catalyst reaction model

As discussed above, the model of Lee[6] is generally applicable to the catalyst reaction model for the decomposition of HAN. In this part, we focus on the difference in the mass spectra obtained under conditions with and without catalyst in order to elucidate the effect of the catalyst on the decomposition of HAN. Mass spectra obtained at 300 °C with catalyst, and at 200 °C with/without catalyst, are shown in Figure 6 and Figure 7, respectively. Figure 6 displays few peaks, and this observation could be due to the overall transformation preferring to produce N_2 and H_2O in the presence of catalyst.

Although the catalyst promotes the reaction by decreasing the overall activation energy, there may be a very high energy barrier between the reactants and products. In other words, it seems unlikely that the catalyst guides the reaction directly toward to N_2 and H_2O. Therefore, we considered that adsorption might be important in this experiment. All samples were diluted to protect the analyzer; therefore, unreacted components remain on the catalyst during the decomposition reaction. Adsorption is classified into two types: physical and chemical. In both type, mobility increases as the temperature is increased. Using this fact, we can construct a hypothesis in which decomposition gases are adsorbed onto the unreacted catalyst and, therefore, do not appear in the corresponding mass spectra. This hypothesis requires further consideration.

At 200 °C without catalyst, we can see similar mass peaks, like *m/z* 18, 30, 32 and 33 (Figure 7(a)). On the other hand, NO_2 and HNO_3 peaks were not observed on mass spectrum. These reasons are for temperature decreasing from 300 °C to 200 °C prevented reaction progresses of NO_2 and HNO_3 generation, or accelerated consumption of NO_2 and HNO_3. When Figure 7(b) is compared to Figure 6 and Figure 7(a), at 200 °C the peak at around *m/z* 30 has decreased in intensity, while a peak at *m/z* 44 has appeared, clearly demonstrating that the catalyst has affected this reaction. The *m/z* 44 peak appears to correspond to N_2O, from its chemical structure, $N_xH_yO_z$. The FHWM is similar to those discussed previously, indicating that this peak might correspond to a molecular ion. On the other hand, peaks at *m/z* 30 and 33 were not observed. According to the model of Lee, N_2O comes from the reaction between NH_2OH and HONO, or the decomposition of HNO, through HNO-HNO. In the same way, NO comes from the decomposition of HONO, through HONO-HONO. Furthermore, the peak for NH_2OH was observed to decrease in the presence of the catalyst. In consideration of these facts, we expected that the catalyst facilitates the reaction between NH_2OH and HONO. We have previously reported that the catalyst affects the first step of HAN decomposition[31], or the reaction between NH_2OH and HNO_3[32]. These results show that catalyst operates on multiple reactions during the decomposition of HAN. Consequently, further knowledge about the mechanism of HAN decomposition is important.

4. Conclusion

In this study, we focused on discussing two topics with the aid of an MPI/TOF-MS simulated thruster system.

Thermal decomposition model

By MPI/TOF-MS analysis, we were able to confirm the major chemical species reported in a conventional thermal decomposition model. Our analyses show that this model is useful and reasonably applicable for the catalyst reaction model. We also found new species that have not been reported previously. We need to consider and investigate reactions to explain the appearance of these new species.

Investigation into the catalyst reaction model

We demonstrated the effect of the S405 catalyst during HAN decomposition and propose that the catalyst facilitates the reaction between NH_2OH and HONO. This result is new and different from other reports made by us. These results are useful for the further development of thrusters and catalysts for thruster systems.

Acknowledgement

This research was supported by the liquid propellant group of the Japan Aerospace Exploration Agency. Experiments were conducted in the Imasaka laboratory at Kyushu University. We thank Kentaro Kojima and Sinpei Shibuta for helpful experiments and discussion.

References

1) G. P. Sutton and O. Biblarz, "Rocket Propulsion Elements", Eighth Ed., John Wiley & Sons, Hoboken (2010).
2) T. Katsumi, T. Inoue, and K. Hori, Sci. Tech. Energetic Materials, 74, 1–5 (2013).
3) R. Amrousse, T. Katsumi, N. Azuma, K. Hatai, H. Ikeda, and K. Hori, Sci. Tech. Energetic Materials, 77, 105–110 (2016).
4) H. S. Lee and T. A. Litzinger, Combust. Flame, 135, 151–169 (2003).
5) R. Amrousse, T. Katsumi, Y. Niboshi, N. Azuma, A. Bachar, and K. Hori, Appl. Catal. A–Gen., 452, 64–68 (2013).
6) R. Amrousse, T. Katsumi, N. Itouyama, N. Azuma, H. Kagawa, K. Hatai, H. Ikeda, and K. Hori, Combust. Flame, 162, 2686–2692 (2015).
7) N. Klein, Proc. 27th JANNAF Combustion Subcommittee Meeting, 557, 443–450 (1990).
8) J. W. Schoppelrei and T. B. Brill, J. Phys. Chem. A, 101, 8593–8596 (1997).
9) J. W. Schoppelrei, M L. Kieke, and T. B. Brill, J. Phys. Chem. A, 100, 7463–7470 (1996).
10) K. I. Hadjiivanov, Catal. Rev., 42, 71–144 (2000).
11) R. H. Tourin, P. M. Henry, and E. T. Liang, J. Opt. Soc. Am., 51, 800–801 (1961).
12) L. D. Barron and A. D. Buckingham, Mol. Phys., 20, 1111–1119 (1971).
13) Å. Bergman, E. K. Wehler, H. Kuroki, and A. Nilson, Chemosphere, 30, 1921–1938 (1995).
14) R. A. Friedel, J. L. Shultz, and A. G. Sharkey, Anal. Chem., 31, 1128 (1959).
15) T. Uchimura, Bunseki Kagaku, 58, 126 (2009). (in Japanese).
16) T. Uchimura, Y. Sakoda, and T. Imasaka, Anal. Chem., 80, 3798–3802 (2008).
17) R. Ezoe, T. Imasaka, and T. Imasaka, Anal. Chim. Acta, 853, 508–513 (2015).
18) A. Hamachi, T. Okuno, T. Imasaka, Y. Kida, and T. Imasaka, Anal. Chem., 87, 3027–3031 (2015).
19) N. Itouyama, T. Matsui, S. Yamamoto, T. Imasaka, and T. Imasaka, J. Am. Soc. Mass Spectrom., 27, 293–300 (2015).
20) Y. Tang, T. Imasaka, S. Yamamoto, and T. Imasaka, Chemosphere, 152, 252–258 (2016).
21) T. Katsumi, H. Kodama, T. Matsuo, H. Ogawa, N. Tsuboi, and K. Hori, Combust. Explos. Shock Waves, 45, 442–453 (2009).
22) J. Matsumoto, B. Nakano, and T. Imasaka, Anal. Sci., 19, 383–386 (2003).
23) J. Matsumoto, G. Saito, and T. Imasaka, Anal. Sci., 18, 567–570 (2002).
24) H. Tsukatani, H. Okudaira, O. Shitamichi, T. Uchimura, and T. Imasaka, Anal. Chim. Acta, 682, 72–76 (2010).
25) R. Amrousse, K. Hori, W. Fetimi, and K. Farhat, Appl. Catal. B–Environ., 127, 121–127 (2012).
26) E. A. Bruns, V. Perraud, A. Zelenyuk, M. J. Ezell, S. N. Johnson, Y. Yu, D. Imre, B. J. Finlayson-Pitts, and M. L. Alexander, Environ. Sci. Technol., 44, 1056–1061 (2010).
27) A. Stirling, I. Pápai, J. Mink, and D. R. Salahub, J. Chem. Phys., 100, 2910–2923 (1994).
28) D. M. Smith, W. F. Welch, S. M. Graham, A. R. Chughtai, B. G. Wicke, and K. A. Grady, Appl. Spectrosc., 42, 674–680 (1988).
29) E. D. Glendening and A. M. Halpern, J. Chem. Phys., 127, 164307 (2007).
30) A. Joseph and S. Sharma, "IIT JEE Super Course in Chemistry: Inorganic Chemistry", Pearson Education India, Chennai (2012).
31) N. Yosui, T. Shiroki, T. Katsumi, R. Amrousse, N. Azuma, and K. Hori, Proc. 9th Symposium on High Energy Materials (HEMs), HEMs–07 (2013).
32) R. Amrousse, T. Katsumi, A. Bachar, E. Brahmi, M. Bensitel, and K. Hori, Reac. Kinet. Mech. Cat., 111, 71–88 (2014).